Mechanosynthesis of bcc alloys from Fe50–y/2Co50–y/2Sn y mixtures ($2 \leq y \leq 33$) and B2 ordering by annealing at modest temperatures

B. F. O. Costa, B. Malaman, Gérard Le Caër, P. M. M Gordo, A. Ramalho

Hyperfine Interactions (2017) 238:76 (13 pages)

https://doi.org/10.1007/s10751-017-1453-3

Mechanosynthesis of bcc alloys from $Fe_{50-y/2}Co_{50-y/2}Sn_y$ mixtures ($2 \leq y \leq 33$) and B2 ordering by annealing at modest temperatures

B.F.O. Costa[1], B. Malaman[2], G. Le Caër[3], P.M. Gordo[1] and A. Ramalho[4]

[1] *CFisUC, Physics Department, University of Coimbra, 3004-516 Coimbra, Portugal*
[2] *Institut Jean Lamour, Département P2M, Equipe 103, CNRS (UMR 7198)- Université de Nancy, B.P. 70239, 54506 Vandoeuvre-les-Nancy Cedex, France*
[3] *Institut de Physique de Rennes, UMR URI-CNRS 6251, Université de Rennes I, Campus de Beaulieu, Bat 11A, 35042 Rennes Cedex, France*
[4] *CEMUC, Department of Mechanical Engineering, University of Coimbra, 3000-272 Coimbra, Portugal*

Abstract

Elemental powder mixtures of Fe, Co and Sn of initial compositions $Fe_{50-y/2}Co_{50-y/2}Sn_y$ ($2 \leq y \leq 26$) are ball-milled at high-energy. They yield metastable alloys which are predominantly composed of a supersaturated bcc Fe-Co-Sn phase. The amount of tin dissolved in it is at least ~15 at.% in the dynamical conditions of milling which were selected. A recently discovered stannide, $CoSn_5$, passed hitherto unobserved in Co–Sn binary phase diagrams. It forms at Co-Sn interfaces at very short milling times, 0.5h, thanks to the high-diffusivity of cobalt in tin. Finally, neutron diffraction and ^{119}Sn Mössbauer spectroscopy show that metastable B2 ordering develops in as-milled alloys, for $y \leq 26$, when they are further annealed at modest temperature, here for 15h at 675K. The tendency to long-range order in ternary Fe-Co-Sn bcc alloys is thus observed in metastable alloys.

Keywords

Mechanical alloying, Fe-Co-Sn alloys, intermetallic compounds, B2 long-range order, Mössbauer spectroscopy, lithium-ion batteries

1. Introduction

Iron-cobalt alloys have exceptional magnetic properties and are mechanically relatively strong [1]. Near-equiatomic $Fe_{100-z}Co_z$ alloys are bcc (A2) below ~1250K [1]. They order to a CsCl type structure (B2) at temperatures below ~1000K for z ranging from ~40 to ~60. Ab initio calculations show that a Co_2FeSn Heusler alloy is unstable relative to other phases but with a small energy difference so that this alloy may be possibly synthesized by non-equilibrium techniques [2]. In connection with possible order-disorder phenomena, we choose to add tin to near-equiatomic FeCo alloys. However, the equilibrium solubility of Sn in FeCo (A2 or B2) is at most ~ 1 at% [3-5]. Therefore, one has to resort to techniques of preparation of metastable alloys, here mechanosynthesis [6-7], to extend significantly the solubility of tin. An additional reason in favour of the choice of tin is related to the formation of iron and of cobalt stannides in the early stages of milling. Indeed, there is a revival of interest in iron and cobalt stannides owing to their potential applications as anode materials of rechargeable lithium-ion batteries (see for instance [8-13]). Both ^{57}Fe and ^{119}Sn Mössbauer spectroscopy are particularly well-suited for a characterization of the alloys all along the mecanosynthesis process as well as in their as-milled and annealed states. Finally, the difference in coherent neutron scattering lengths of Fe (b_{Fe} = 9.45 fm) and of Co (b_{Co}= 2.49 fm) makes neutron diffraction particularly relevant to characterize as-milled and annealed alloys.

We synthesized thus metastable ternary Fe-Co-Sn alloys by mechanical alloying (MA) of elemental powder mixtures, abbreviated as "p", of Fe, Co and Sn whose initial compositions (at.%) are denoted hereafter as p-$Fe_{50-y/2}Co_{50-y/2}Sn_y$ ($2 \leq y \leq 33$) [14-17]. The latter denomination will be used to designate powders milled for times intermediate between 0.5h and ~10h whose compositions have not been measured. The final Sn contents x of powders milled for 10h are a little larger, by less than ~ 1 at.%, than the nominal contents y. Their overall composition is $Fe_{53.3-0.6x}Co_{46.7-0.4x}Sn_x$ (section 2). As-milled powders consist of a single supersaturated bcc phase for x <~15 at.%. For larger values of x, they are primarily composed of a bcc phase, whose tin content still increases up to ~26 at.%, and of extra phases, which include hexagonal $(Fe,Co)_3Sn_2$ of the $B8_2$ type.

In the present paper, we begin with a summary of our previous results on the overall evolution of ternary powder mixtures with milling time and on the structure of as-milled

ternary alloys. Mechanical alloying of these ternary alloys gives birth to materials of interest, either at short milling times or by further processing of as-milled alloys. Then, we focus on Co-Sn stannides, which form transiently in the first stage of milling, in the light of recent experimental and theoretical literature results [9-12]. Finally, we place emphasis on the complementary roles of ^{119}Sn Mössbauer spectroscopy and of neutron diffraction to evidence B2 ordering of as-milled bcc alloys when they are annealed at modest temperatures.

2. Experimental

Elemental powder mixtures of Fe (purity: 99.9%), Co (purity: 99.8%) and Sn (purity: 99.5%) were ball-milled in argon atmosphere in a planetary Fritsch P6 ball-mill at 500 rpm whose vials and balls of 15 mm diameter (seven), are made of hardened steel. The powder-to-ball weight ratio was 1:20. Hereafter, unless otherwise stated, "as-milled" denotes powder mixtures ground for 10h in these dynamical conditions.
Scanning electron microscopy (SEM) images and X-ray maps (Fe, Co, Sn) were obtained in a in a JEOL JSM630 microscope, working at 15kV. The compositions of as-milled powders deviate from their starting compositions, p-$Fe_{50-y/2}Co_{50-y/2}Sn_y$. They were determined by energy-dispersive X-ray spectroscopy (EDS: Oxford Inca Energy 35) in a standard analysis with 20 keV electron beam. The Sn content x of powders milled for 10h is given by $x = 1.05y-0.16$ with an accuracy better than 0.2 at.% for $2 \leq y \leq 25$ while $x = 34$ for $y = 33.3$. Due to contamination by iron from milling tools, the Fe content is found to be larger than its nominal content while the reverse holds for Co. The resulting composition of as-milled alloys is finally well described by $Fe_{53.3-0.6x}Co_{46.7-0.4x}Sn_x$ with Fe and Co contents accurate to within ~0.3 at.% for $2 \leq x \leq 26$ [17]. The alloy composition is $Fe_{34.7}Co_{31.3}Sn_{34}$ for $x = 34$. For simplicity, any alloy is designated hereafter by Fe, Co, and Sn contents rounded to the nearest integers, for instance $Fe_{35}Co_{31}Sn_{34}$ for the latter alloy.

As-milled powders were placed in quartz tubes which were first evacuated by a primary pump and were then filled with argon. These two steps were repeated ten times before sealing the tubes under an argon pressure of about 27 kPa at 300K. As-milled alloys were finally annealed at 673K for 15h.

As-milled and annealed alloys were characterized by X-ray diffraction (XRD), ^{57}Fe and ^{119}Sn Mössbauer spectroscopy. X-ray diffraction patterns were measured using CuKα radiation (λ = 0.1542 nm). Annealed alloys were further studied by neutron diffraction (ND) at Institut Laue Langevin (ILL, Grenoble, France), with the one-dimensional multidetector D1B (λ =0.252 nm). The coherent scattering lengths for neutron diffraction are b_{Fe} = 9.45 fm, b_{Co}= 2.49 fm, b_{Sn} = 6.225 fm, b_O = 5.803 fm for Fe, Co, Sn and O respectively.

^{57}Fe and ^{119}Sn Mössbauer spectra were recorded at room temperature (RT) in transmission geometry, by a constant acceleration type spectrometer using sources of ^{57}Co in Rh and ^{119m}Sn in $CaSnO_3$ both with a strength of ~ 10 mCi. Hyperfine magnetic field distributions (HMFD's), $P_x(B)$, were analyzed both for ^{57}Fe and ^{119}Sn with a constrained Hesse–Rübartsch method [18] employing Lorentz lines. In the previous notation, X is either F or S which stands for ^{57}Fe and ^{119}Sn respectively. This HMFD is such that $P_X(B)dB$, represents primarily the fraction either of iron atoms or of tin atoms whose field lies between B and B+dB. Finally, we define B_{Max} either as the ^{57}Fe HMF for which $P_F(B)$ is maximum when B ranges between ~20 and 40 T or as the ^{119}Sn HMF for which $P_S(B)$ is maximum when B ranges between ~5 and 30 T where the context makes it clear which is which. Typical errors on $<B_X>$ and on B_{Max} are respectively of ~0.3 T and ~0.2 T.

3. Overall evolution of powder mixtures with milling time t_m

3.1 X-ray diffraction

The progress of the mechanochemical reaction which takes place for an initial tin content of 6 at.% [14] was found to be similar to the one reported below for a content of 12 at.%. The evolution of the latter mixture with milling time t_m is representative too of phenomena which occur for concentrated ones. X-ray maps of Fe, Co and Sn recorded for typical particles (≈ 30 μm) of p-$Fe_{44}Co_{44}Sn_{12}$ showed that the elements are not yet distributed homogeneously after 1h30 of milling (similar maps were obtained for p-$Fe_{47}Co_{47}Sn_6$ milled for 1h as shown by figure 1 of [14]). By

contrast, Fe, Co and Sn were seen to be homogeneously distributed in powder particles milled for t_m > ~8h.

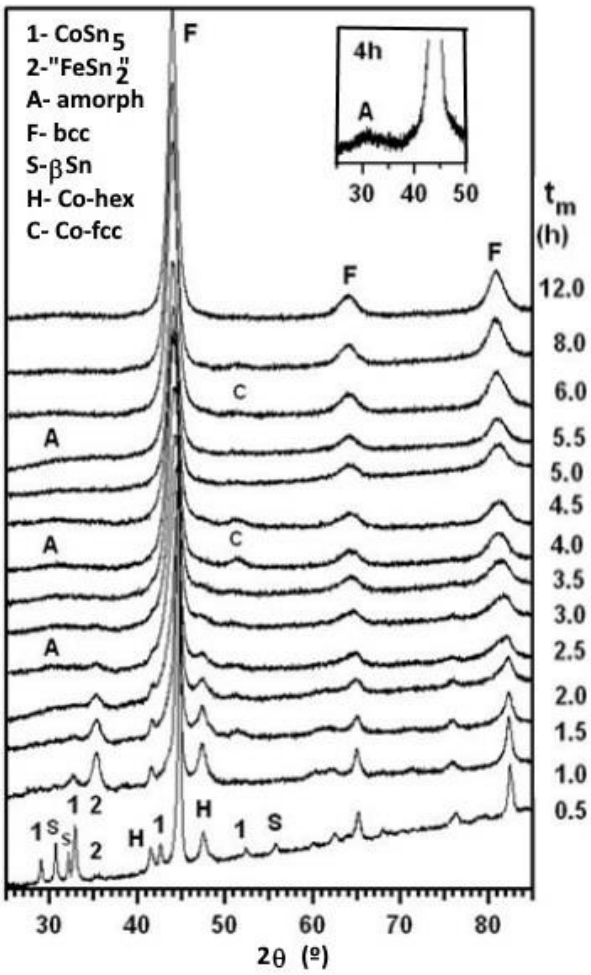

Figure 1- Evolution with milling time, t_m (indicated on the right), of the XRD patterns of mechanically alloyed p-$Fe_{44}Co_{44}Sn_{12}$ [16].

The structural evolution of p-$Fe_{44}Co_{44}Sn_{12}$ powders with milling time was followed by XRD (figure 1). Diffraction peaks are broad, as expected, because of strains and of nanometer grain sizes. A bcc phase is well evidenced (F, fig. 1). Figure 2 shows the milling time dependence of the lattice parameter of the bcc phase. The mecanosynthesis process is composed of two main steps. In the first step, for milling times ranging from 0.5h to 2h, the lattice parameter remains essentially constant. As shown in Fig. 1 and as further discussed in section 4, this milling period is characterized by the formation of

stannides. The second step occurs for milling times $t_m \geq 2.5$h until a stationary state is reached at ≈ 8h. Stannides formed during the first step dissolve gradually and the composition of the ternary bcc alloy evolves progressively to the final one [16]. For milling times ranging from 8 to 16h, the lattice parameter remains essentially constant a result which holds for the various tin contents we studied [15]. A milling time of 10h, a time sufficiently long for the milled powders to reach a stationary state but not too long to avoid an excessive contamination, was finally chosen to prepare the studied alloys.

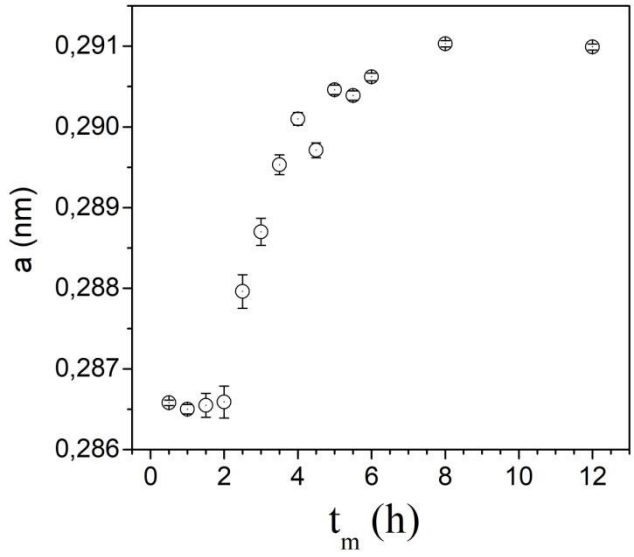

Figure 2- Evolution with milling time, t_m, of the lattice parameter of the bcc phase of mechanically alloyed p-$Fe_{44}Co_{44}Sn_{12}$ as calculated from XRD patterns of figure 1.

In our global milling conditions, the maximum solubility of Sn in bcc $Fe_{53.3-0.6x}Co_{46.7-0.4x}Sn_x$ is concluded to be 15 ± 2 at% considering that no extra peaks are visible on XRD patterns and on ^{119}Sn Mössbauer spectra up to this Sn content [17]. The equilibrium solubility of Sn in near-equiatomic Fe-Co is recalled to be less than 1 at%. For x > 15 at%, the lattice parameter of the bcc phase continues however to increase regularly with Sn content even when other phases coexist with it. The latter phase coexistence is made possible because high-energy ball-milled materials are generally, as here, in dynamical equilibrium [6] which differs in most cases from thermodynamical equilibrium. Above 15 at% Sn a two-phase region (bcc + amorphous) exists up to ≈ 26 at%, in which polymorphs have the same composition. The amorphous phase is partly

decomposed into hexagonal $(Fe,Co)_3Sn_2$ of the $B8_2$ type and into a bcc Fe-Co alloy (fig. 1 of [17]).

3.2 Characterization of as-milled alloys by Mössbauer spectroscopy

Figure 3 shows RT ^{57}Fe and ^{119}Sn Mössbauer spectra of alloys milled for 10h. Diamagnetic Sn reduces the average Fe hyperfine field when dissolved in bcc FeCo as it does in bcc Fe. The RT ^{119}Sn Mössbauer spectra consist of a magnetic component with two broad unresolved lines. With the increasing of Sn content, particularly for $x > 15$, a central non-magnetic component appears. The mean ^{119}Sn hyperfine field remains almost constant with Sn content up to about 15 at%: $\langle B_S(x)\rangle$=9.5(0.3) T. It is 8.5 T for x = 21 [17]. ^{57}Fe Mössbauer spectra strengthen the conclusion drawn from XRD patterns that as-milled alloys mainly consist of bcc Fe-Co-Sn alloys.

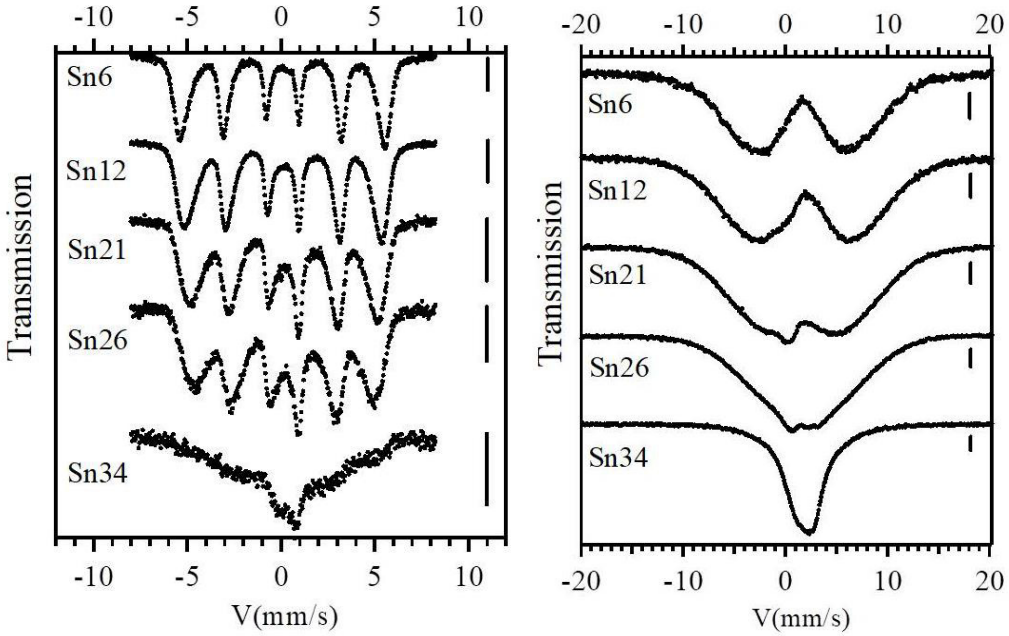

Figure 3- Room temperature ^{57}Fe (left) and ^{119}Sn (right) Mössbauer spectra of $Fe_{53.3-0.6x}Co_{46.7-0.4x}Sn_x$ milled for 10 h [17] (every vertical bar represents 1% and 2% absorption for ^{57}Fe and ^{119}Sn respectively).

After having recalled how Fe-Co-Sn mixtures are progressively mechanosynthesized to yield metastable bcc alloys, we go back first on the cobalt stannide $CoSn_5$ which is formed in the early stage of mechanical alloying for all investigated compositions.

4. Transient formation of $CoSn_5$ at short milling times

For milling times as short as those considered below, compositions are expected to remain essentially unchanged and equal to the nominal ones. Fig. 4 shows selected X-ray maps of Fe, Co and Sn for a typical particle (≈ 30 μm) of $Fe_{44}Co_{44}Sn_{12}$ milled for 0.5h in which these elements are distributed heterogeneously. Cobalt and iron regions almost depleted of Sn, are observed. Co-rich zones include "ovals" of different sizes as well as elongated and flattened zones. Fe-rich zones are on the whole elongated and correspond to the typical description of ball-milled ductile particles [6-7]. Sn-rich zones differ from the previous ones: Co and Fe regions seem to be embedded within tin regions.

During collisions between balls or between a ball and the vial wall, powder particles are trapped and subjected to high stresses for times of the order of microseconds. During shocks, the temperature of a trapped volume of powders increases. We denote the representative temperature increase with respect to ambient temperature by ΔT. The repeated fracturing, flattening and rewelding processes of ductile powder particles, which occur during shocks, mix elements in a way reminiscent of chaotic transformations of the 'baker' type [6]. In that way, relevant sizes of solids to be mixed decrease rapidly down to the nanometer scale. The impact speed is of the order of several $m.s^{-1}$ and shock frequencies are several hundred Hz. The waiting period between effective trapping events is usually of the order of tens to hundreds of seconds [6]. Temperature rises of typical powder alloys milled in a shaker *Spex 8000* ball-mill were estimated to be $\Delta T \leq 350K$ using computer models and experiments [19]. Planetary ball-mills have dynamical features which overlap those of vibratory mills and extend possibly to more energetic characteristics, for instance larger kinetic energies per shock. The melting temperature of Sn is 505 K, i.e. $\Delta T = 505\text{-}295=210K$. Thus, tin might be molten when trapped with Co and Fe particles. This is in fact the case when p-$Cr_{90}Sn_{10}$ mixtures are ball-milled in a *Spex 8000* with WC milling tools [20]. Indeed,

micrographs show undoubtedly that the lamellar structures, which are observed to form initially when ball-milling ductile materials, are created from chromium and from molten tin (figure 4, top right). Tin melting followed by cooling down to the temperature of the interior of the vial would help to interpret the (Co+Fe+Sn) X-ray map of fig. 4 with its numerous Co-Sn and Fe-Sn interfaces. Some Fe-Co interfaces are also observed.

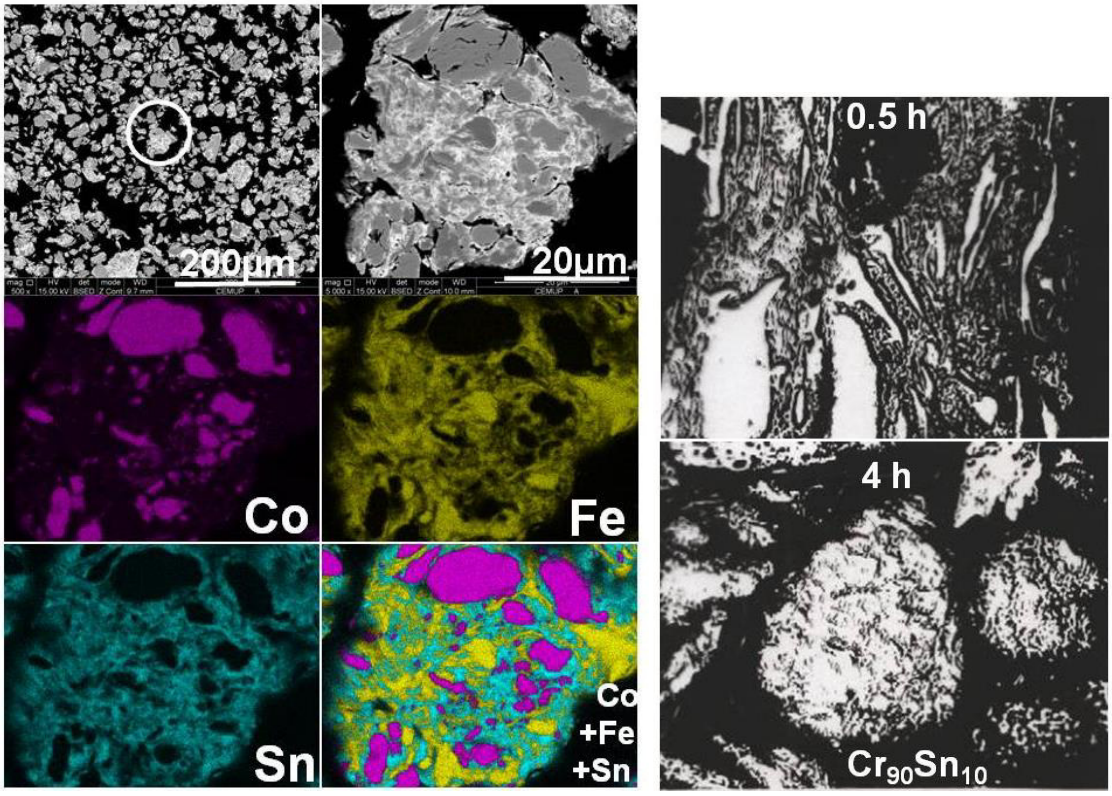

Figure 4- left part: SEM micrographs of p-$Fe_{44}Co_{44}Sn_{12}$ milled for 0h30: overall view (top) and an enlarged view of the circled particle; Co, Fe, Sn, Co+Fe+Sn X-ray maps of the previous particle; right part: SEM micrographs of p-$Cr_{90}Sn_{10}$ milled for 0.5h (top) and for 4h (bottom) [20].

The first stage, for $0.5 \leq t_m \leq 2h$, is characterized by the formation of two stannides, first $CoSn_5$ and then $FeSn_2$, respectively at Co-Sn and Fe-Sn interfaces. The most intense lines at t_m=0.5 h, (‘1’ in Fig. 1) as well as additional other lines which are not seen at the scale of the figure, are due to ‘‘$CoSn_5$’’ [16], a recently discovered stannide possibly non-stoichiometric ($Co_{1-z}Sn_5$, z=0.1–0.2) [10]. Nanospheres of $CoSn_5$

were synthesized through a conversion chemistry route [10]. Here, it is formed transiently by mechanical alloying and disappears after ~1.5h milling. "$CoSn_5$" is tetragonal (P4/mcc space group) with a single crystallographic site (2(c)) for Co atoms. Tin occupies two non-equivalent crystallographic sites, Sn1 (position 2(b)) and Sn2 (position 8(m)). There are thus four Sn2 for one Sn1. The reported lattice parameters are a=b=0.69328 nm, c=0.57924 nm [10]. The second stannide ('2' in Fig. 1) is tetragonal $FeSn_2$ with a $CuAl_2$ type structure (I4/mcm space group with a=b=0.6539 nm, c=0.5325 nm). The decrease of the most intense XRD peak of $FeSn_2$ starts at t_m ~ 2 h but it is still seen at t_m=3 h. Tetragonal $FeSn_2$ forms too during the first stage of mechanical alloying of Fe-Sn alloys [21-22].

Cobalt stannide formed by MA of ternary Fe-Co-Sn mixtures does not contain iron as confirmed by neutron diffraction patterns. Consistently, $CoSn_5$ does not contribute to ^{57}Fe Mössbauer spectra. XRD patterns show that $CoSn_5$ forms too in the early stage of MA of Co–Sn alloys at any Sn content ranging between 6 and 83 at.%. ^{119}Sn Mössbauer spectra of $Co_{88}Sn_{12}$ and of $Fe_{44}Co_{44}Sn_{12}$, both milled for t_m = 0.5 h, share similar features as seen in fig. 5 which shows spectra of p-$Fe_xCo_{88-x}Sn_x$ (t_m=0.5 h, x=0, 44, 88) recorded at RT. Both differ strongly from the spectrum of p-$Fe_{88}Sn_{12}$, despite the fact that $FeSn_5$ isostructural with $CoSn_5$ does exist too [9]. A broad component centered at ~0.8 mm/s is indeed missing in the range -1,+1mm/s of the spectrum of p-$Fe_{88}Sn_{12}$. The β-Sn spectrum at RT consists of a broadened line (Γ ~ 1 mm/s) with an isomer shift of 2.52 ± 0.03 mm/s and a quadrupole splitting of 0.41±0.04 mm/s ([23] and references therein, [24]).

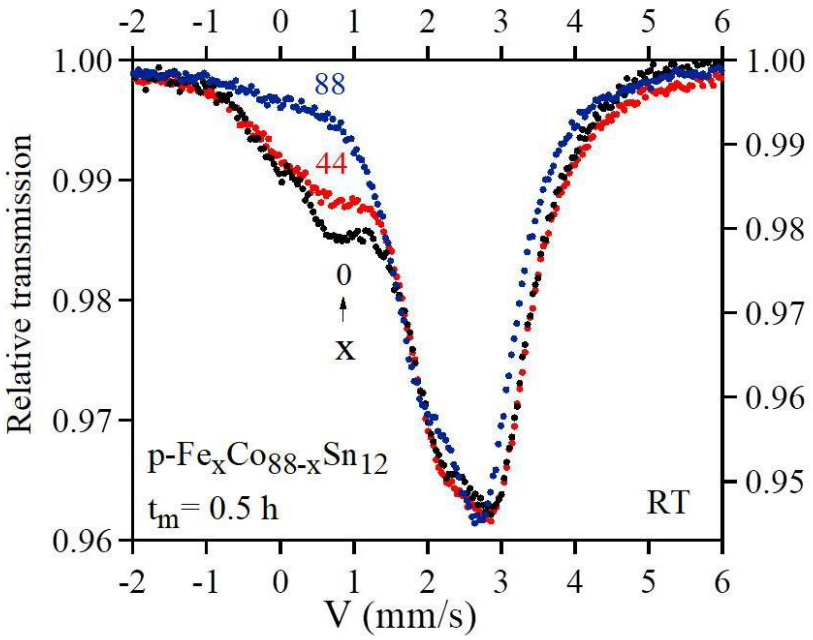

Figure 5- Room temperature ^{119}Sn Mössbauer spectra of elemental powder mixtures of composition p-$Fe_xCo_{88-x}Sn_{12}$ milled for 0.5h (x=0, 44, 88).

The contributions of $CoSn_5$ to the spectra of fig. 5 are strongly enhanced at RT as the recoil-free fraction of the main phase, β-Sn, is only of 0.06 ± 0.01 while it is 0.715 ± 0.01 at 10K [23, 25]. The relative contribution of $CoSn_5$ is indeed seen to decrease significantly for p-$Fe_xCo_{88-x}Sn_x$ spectra recorded at 15K (t_m=0.5 h, x=0, 44) which confirm in addition that $CoSn_5$ is non-magnetic as are all tin-rich cobalt stannides. Reliable hyperfine parameters of $CoSn_5$, recalled to be likely non-stoechiometric, are however difficult to obtain owing to the possible existence, besides β-Sn, of Sn environments in other phases, for instance in $FeSn_2$ for x=44 (fig. 1). The formation of the latter phase explains, for x=0, the slope of the Mössbauer spectrum between 0 and 1 mm/s (fig. 5 and figure 4 of [26]).

Formation enthalpies of $FeSn_5$ and of $CoSn_5$ were obtained recently by first-principles calculations [12]. Sun et al. concluded that the enthalpies of formation of $FeSn_5$ and of $CoSn_5$ are both negative, respectively -0.067 and -0.088 eV/atom for Fe and Co. The formation enthalpies they obtained for $FeSn_2$ and $CoSn_2$, respectively -0.148 and -0.177 eV/atom, are significantly smaller than the previous values. They might in part explain why MSn_5 passed unobserved until now in M–Sn binary phase diagrams (M=Fe,Co) [12]. Kinetic factors might also come into play.

Questions are thus raised by the different behaviors of Co-Sn and Fe-Sn at interfaces during the early stage of mechanosynthesis: why does $CoSn_5$ forms first instead of $CoSn_2$ or why does $FeSn_2$ forms first instead of $FeSn_5$?

These differences are likely explained by kinetic factors, namely by the fact that Co is an anomalously fast diffuser into Sn. The high Co diffusivity accounts for the formation at RT of amorphous Co_xSn_{1-x} alloys ($\sim 0.2 \leq x \leq \sim 0.6$) from polycrystalline multilayers (~ 6 nm) of Co and Sn deposited at 77 K [27]. The interdiffusion coefficient is of the order 10^{-22} m^2/s at RT [27]. In the present case, the Co diffusivity is further enhanced because of the pulse of temperature which occurs during shocks and during the subsequent cooling step between trapping events, a fact which makes possible the fast formation of $CoSn_5$.

5. Ordering of as-milled alloys by annealing at modest temperatures

$Fe_{53.3-0.6x}Co_{46.7-0.4x}Sn_x$ as-milled alloys were annealed for 15h, under argon atmosphere, at a selected temperature of 673 K [17].

5.1 Characterization of annealed alloys by neutron diffraction

Figure 6 shows neutron diffraction patterns for such alloys with $6 \leq x \leq 26$. They reveal the presence of (100) and (111) superlattices lines. Diffraction lines of a $CoFe_2O_4$ oxide are also seen. The presence of superlattice lines (hkl), with h + k + l odd, establishes that the bcc phases of as-milled alloys transform, for $x \leq 26$, into long range ordered B2 phases by annealing at 673 K. In the as-milled state, the crystallite size is ≈ 6 nm [15]. We estimated that the mean crystallite size and the mean size of ordered domains in annealed alloys are ≈ 10 nm and ≈ 4 nm, respectively [17].

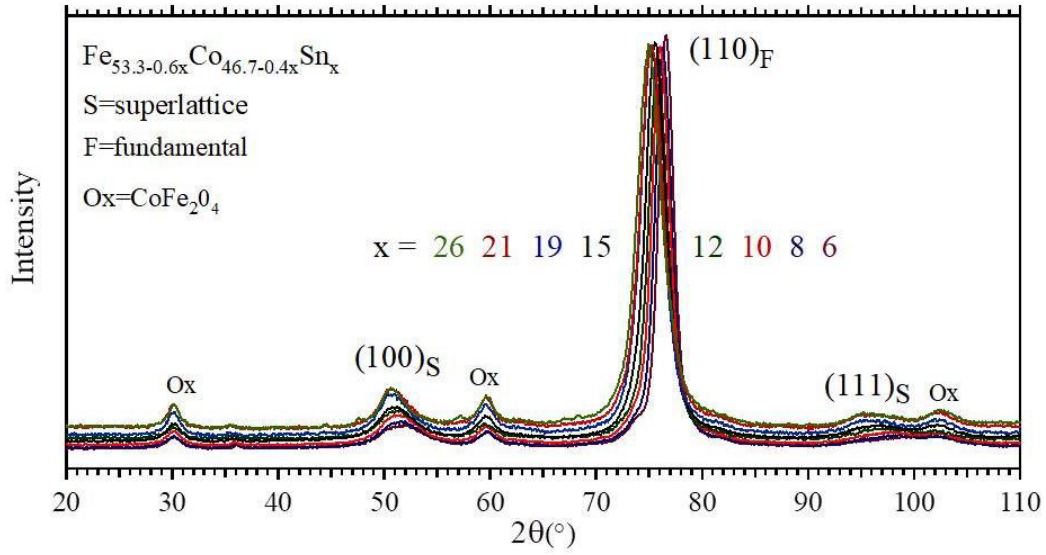

Figure 6 - Neutron diffraction patterns (λ =0.252 nm) of as-milled $Fe_{53.3-0.6x}Co_{46.7-0.4x}Sn_x$ alloys ($6 \leq x \leq 26$) annealed at 673K for 15h. [17].

5.2 Characterization of annealed alloys by Mössbauer spectroscopy

RT ^{57}Fe Mössbauer spectra of as-milled $Fe_{53.3-0.6x}Co_{46.7-0.4x}Sn_x$ annealed at 675K for 15h are shown in figure 7 of [17]. The formation of $CoFe_2O_4$, evidenced by neutron patterns (fig. 6), is confirmed by small peaks at ≈ 8 mm/s [17, 28]. For x = 34, as-milled alloys decompose during annealing. The ^{57}Fe spectra do not change much with annealing for $x \leq 26$. Lines (fig. 3) become thinner [17] with little change of average hyperfine parameters as exemplified by figure 7 (left) which shows the room-temperature HMFD's, $P_F(B)$, of $Fe_{46}Co_{42}Sn_{12}$ both in the as-milled and in the annealed states. The average ^{57}Fe HMFD's of the latter alloys are respectively 31.7 T and 32.9 T. The mean ^{57}Fe hyperfine field of as-milled alloys, $\langle B_F(x)\rangle$, decreases fairly linearly with Sn content, $\langle B_F(x)\rangle$ (T) = 34.7-0.25x ($4 \leq x \leq 26$). The field B_{Max} at which a ^{57}Fe HMFD, $P_F(B)$, reaches its maximum is close to $\langle B_F(x)\rangle$ and varies also linearly $B_{Max}(x)$ (T) = 35-0.19x ($4 \leq x \leq 26$) [17]. For annealed alloys (figure 7, right) , it comes $\langle B_F(x)\rangle$ (T) = 34.1-0.10x ($4 \leq x \leq 26$) while $B_{Max}(x)$ (T) = 34.5-0.11x ($4 \leq x \leq 15$) and $B_{Max}(x)$ (T) = 32.6 ($x > 15$). ^{57}Fe Mössbauer spectroscopy is in fine concluded to be rather insensitive to long-range chemical order in these alloys. Beyond long-range order, ^{57}Fe Mössbauer spectra provides a first evidence that the tin content, ~15 at.%, marks the separation between domains with different characteristics, namely Sn short-range order as discussed in detail in [17].

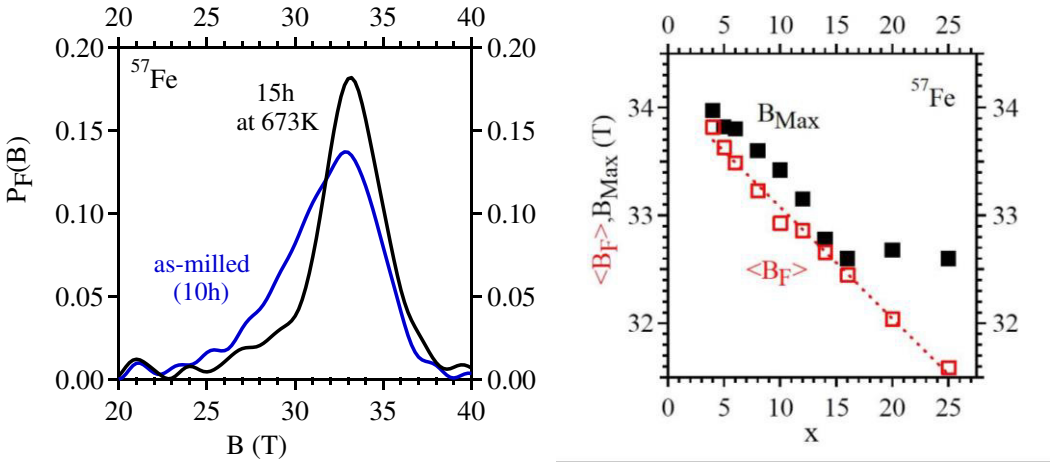

Figure 7- left: RT ^{57}Fe HMFD's of as-milled and of as-milled and annealed $Fe_{46}Co_{42}Sn_{12}$; right: evolution with tin content of the ^{57}Fe mean hyperfine magnetic field $<B_F>$and of the hyperfine magnetic field B_{Max} for annealed alloys.

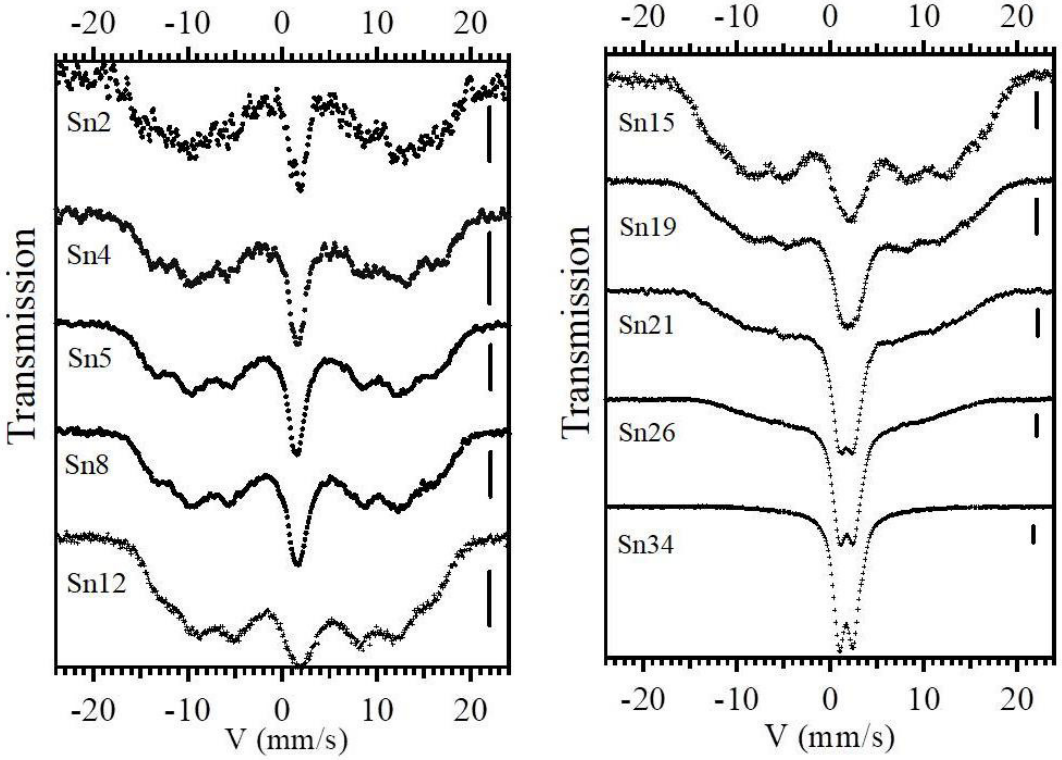

Figure 8- RT ^{119}Sn Mössbauer spectra of as-milled and annealed $Fe_{53.3-0.6x}Co_{46.7-0.4x}Sn_x$ (samples milled for 10 h are further annealed at 675K for 15h) (every vertical bar represents 1% absorption except for Sn2 where it represents 0.1%)

By contrast, ^{119}Sn spectra vary strongly when as-milled alloys (fig. 5 right) are annealed at 675K (fig. 8). A broad magnetically split sextet is observed, being almost unchanged for $x \leq 15$. A central component is also observed. ^{119}Sn hyperfine magnetic fields show a strong sensitivity to chemical order when dissolved in B2 FeCo (table 1). The ^{119}Sn fields of the Co sublattices are much larger than those measured at RT for tin in hcp Co or in fcc Co, 3.6T [29] and 1.7T [30] respectively or in any cobalt stannide. Similarly, the ^{119}Sn fields of iron stannides at RT are all less than 9T.

Table 1:

Mean ^{119}Sn hyperfine magnetic fields, $\langle B_S \rangle$ (T),

measured at RT in Sn-doped B2 FeCo

B2 alloys	Co sublattice
$Fe_{49.9}Co_{49.9}Sn_{0.2}$	25.2* [3]
$Fe_{49.5}Co_{49.5}Sn_1$	25.3 [4]
$Fe_{47.3}Co_{52.4}Sn_{0.3}$	23.1 [5]
B2 alloy	**Fe sublattice**
$Fe_{49.5}Co_{49.5}Sn_1$	0.7* [3]

** HMF's measured at 77K mentioned to be hardly altered between 77K and RT*

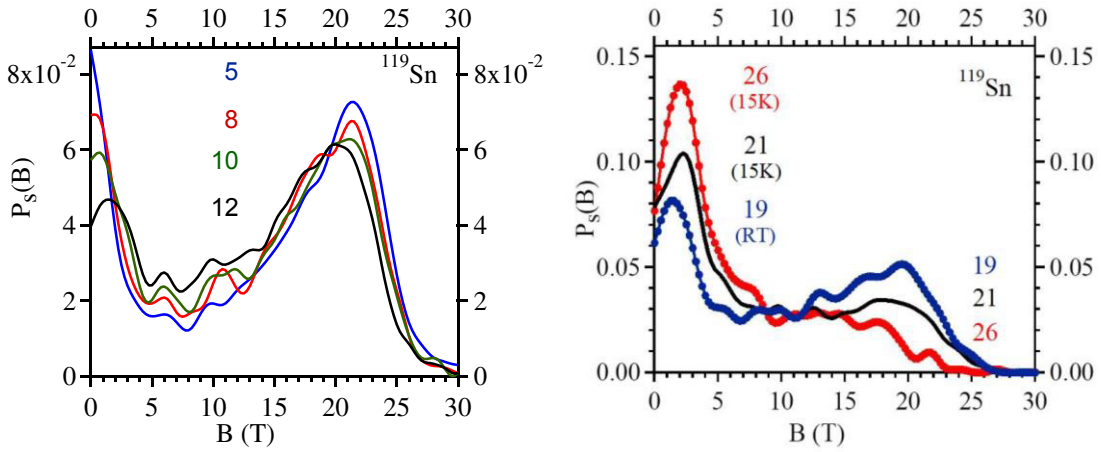

Figure 9- RT ^{119}Sn hyperfine magnetic field distributions of $Fe_{53.3-0.6x}Co_{46.7-0.4x}Sn_x$ for $5 \leq x \leq 26$ (samples milled for 10 h and then annealed at 675K for 15h)

The HMF of tin atoms located on the Fe sublattice is seen to be very small. The central components of spectra (fig. 8, x≤15 at.%) are essentially explained by the contributions of these Sn atoms as further shown by fig. 9 (left). Intense peaks emerge in the ^{119}Sn HMFD's of annealed alloys at values of ≈ 20 T for x ≤ 19 (fig. 9 left). It is necessary to record spectra at low temperatures to evidence peaks at ~18T and 16T for x=21 and 26 respectively (fig. 9 right).

The evolutions with x of $\langle B_S \rangle$ and of B_{Max} are shown in figure 10. The latter field remains close to 20 T for any x ≤ 21. The faster decrease of $\langle B_S \rangle$ for x>15 is related to the increase of the intensity of the peak at small fields (figures 8 and 9 right). The two fields $\langle B_S \rangle$ and B_{Max} coincide for as-milled alloys for which HMFD's are well approximated by Gaussians. The very large increase of B_{Max} between the as-milled and the annealed states can only be interpreted by the development of B2 long-range order in agreement with neutron diffraction results (fig. 6).

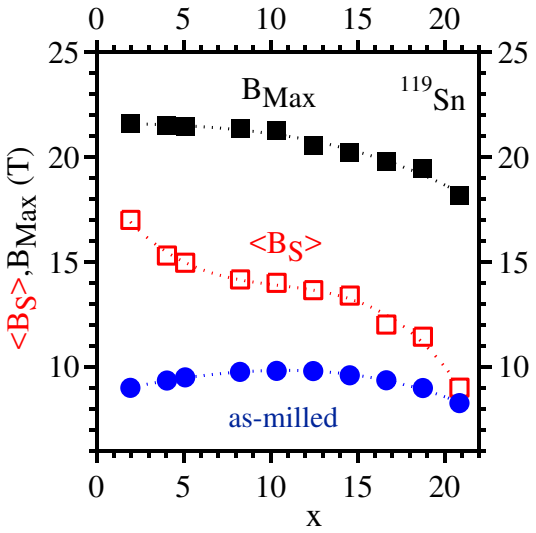

Figure 10- Characteristic hyperfine magnetic fields calculated from RT ^{119}Sn Mössbauer spectra of $Fe_{53.3-0.6x}Co_{46.7-0.4x}Sn_x$ (samples milled for 10 h and then annealed at 675K for 15h)

The fractions of ^{119}Sn atoms, whose hyperfine fields are either less or equal to 5 T or less or equal to 7 T, calculated from HMFD's as a function of Sn content in

$Fe_{53.3-0.6x}Co_{46.7-0.4x}Sn_x$ annealed at 673K for 15h display a change of slope at x ≈ 15 at% (fig. 12 of [17]) suggesting that short-range order of tin atoms evolves with *x* as already indicated by ^{57}Fe spectra (fig. 7 right).

6. Conclusions

First, high-energy ball-milling of elemental powder mixtures of Fe, Co and Sn of initial compositions p-$Fe_{50-y/2}Co_{50-y/2}Sn_y$ ($2 \leq y \leq 33$) yield metastable alloys which are predominantly composed of a supersaturated bcc Fe-Co-Sn phase. The Sn content of all studied alloys is indeed larger than the maximum solubility of ~1 at.% in equilibrium conditions. It can be as large as ~15 at.% in the dynamical conditions of milling which were selected.

Next, a recently discovered stannide, $CoSn_5$, forms at Co-Sn interfaces at very short milling times, 0.5h, thanks to the high-diffusivity of cobalt in tin. Although being an equilibrium phase [12], it passed so far unobserved in Co–Sn binary phase diagrams. Mechanical alloying of Co-Sn elemental powder mixtures provides an additional method of synthesis of this intermetallic compound which would deserve to be further investigated and optimized. Indeed, excellent electrochemical performances were obtained when using MSn_5 (M=Fe,Co, $Fe_{0.5}Co_{0.5}$) stannides as anode materials of rechargeable Li-ion batteries [11].

Finally, neutron diffraction and ^{119}Sn Mössbauer spectroscopy show that metastable B2 ordering develops in as-milled alloys, for $x \leq 26$, when they are further annealed at modest temperatures, here during 15h at 675K. These results confirm that the tendency to long-range order can be observed in ternary Fe-Co-Sn bcc alloys synthesized by non-equilibrium techniques.

Acknowledgements

The financial support of the bilateral Portuguese-French program FCT-CNRS is gratefully acknowledged. We thank ILL for the provision of neutron beam time.

References

[1] Sourmail T., Prog. Mater. Sci. **50**, 816 (2005)

[2] Yin M., Hasier J. and Nash P., J Mater Sci **51**, 50 (2016)

[3] Delyagin N.N. and Kornienko E.N., Sov. Phys. Solid State **13**, 1254 (1971)

[4] Huffman G.P. and Dunmyre G.R. AIP Conf. Proc. **10**,1361 (1973)

[5] Campbell C.C.M., Schaf J. and Zawislak F.C. J Magn Magn Mater **8**,112 (1978)

[6] Gaffet E., Bernard F. Niepce J.C., Charlot F., Gras C., Le Caër G., Guichard J.L., Delcroix P., Mocellin A., Tillement O., J. Mater. Chem. **9**, 305 (1999)

[7] Suryanarayana C., Prog. Mater. Sci., **46**, 1 (2001)

[8] Chamas M., Lippens P-E., Jumas J-C., Hassoun J., Panero S., Scrosati B., Electrochimica Acta **56**, 6732 (2011)

[9] Wang X-L., Feygenson M., Chen H., Lin C-H., Ku W., Bai J., Aronson M.C., Tyson T.A. and Han W.QJ. , Amer. Chem. Soc. **133**, 11213 (2011)

[10] Wang X.L., Chen H., Bai J. and Han W.Q. , J. Phys. Chem. Lett. **3**, 1488 (2012)

[11] Xin F., Wang X., Bai J., Wen W., Tian H., Wang C. and Han W., J. Mater. Chem. A **3**, 7170 (2015)

[12] Sun W., Zhang L., Liu J., Wang H. and Bu Y., Comp. Mater. Sci. **111**, 175 (2016)

[13] Javadian S., Kakemam J., Gharibi H. and Kashani H., Int. J. Hydrogen Energy, **42**, 13136 (2017)

[14] Loureiro J.M., Costa B.F.O. and Le Caër G., J. Alloys Compd. **536S**, S31 (2012)

[15] Loureiro J.M., Costa B.F.O., Le Caër G. and Malaman B., Solid State Phenom **194**, 187 (2013)

[16] Loureiro J.M., Costa B.F.O., Malaman B., Le Caër G., Das S. and Amaral V.S., J. Alloys Compd. **615**, S559 (2014)

[17] Malaman B., Le Caër G. and Costa B.F.O., J. Mater. Sci. **51**, 5775 (2016)

[18] Le Caër G., Dubois J.M., J. Phys. E, **12**, 1083 (1979)

[19] Davis R.M., McDermott B. and Koch C.C., Metall. Trans. A, **19**, 2867 (1988)

[20] de Araujo Pontes L.R., Ph.D. thesis I.N.P.L., Nancy, France (1992)

[21] Cabrera A.F., Sánchez F.H. and Mendoza-Zélis L.A., Phys. Rev. B **53**, 8378 (1996)

[22] Dorofeev G.A. and Elsukov E.P., Inorg. Mater. **36**, 1228 (2000)

[23] Hightower A., Delcroix P., Le Caër G., Huang C-K., Ratnakumar B. V., Ahn C. C. and Fultz B. J., Electrochem. Soc. **147**, 1 (2000)

[24] Svane A., Christensen N.E., Rodriguez C.O. and Methfessel M., Phys. Rev. B **55**, 12572 (1997)

[25] Hohenemser C., Phys. Rev. **139**, A185 (1965)

[26] Le Caër G., Malaman B., Venturini G., Fruchart D. and Roques B., J. Phys. F : Met. Phys. **15**, 1813 (1985)

[27] Guilmin P., Guyot P. and Marchal G., Phys. Lett. **109A**, 174 (1985)

[28] Kovacheva D., Ruskov T., Krystev P., Asenov S., Tanev N., Mönch I., Koseva R., Wolff U., Gemming T., Markova-Velichkova M., Nihtianova D. and Arndt, K.-F., Bulg. Chem. Commun. **44**, 90 (2012)

[29] Jain A.P. and Cranshaw T.E., Phys. Lett. **25A**, 421 (1967)

[30] Cranshaw T.E., J. Appl. Phys. **40**, 1481 (1969)